Facile Synthesis of Ultrathin Two-Dimensional Nanosheets Constructed MCo_2O_4 (M = Ni, Cu, Zn) Nanotubes for Efficient Photocatalytic Oxygen Evolution

Erli Ding[a], Ali Li[a], Hanwen Liu[a], Weisheng Liu[a], Fengjuan Chen[a], Tianrong Li*[a], and Baodui Wang*[a]

State Key Laboratory of Applied Organic Chemistry, Key Laboratory of Nonferrous Metal Chemistry and Resources Utilization of Gansu Province, College of Chemistry and Chemical Engineering, Lanzhou University, Lanzhou, 730000, P. R.

E-mail: litr@lzu.edu.cn; wangbd@lzu.edu.cn.

Experimental Section:

The Valence band maximum (VBM), conduction band minimum (CBM), and the band gap of nanosheets-assembled $CuCo_2O_4$ nanotubes. The intersections of the tangents with the baseline give the edges of the UPS spectra from which the UPS width is determined. As shown in Figure S6, we used ultraviolet photoelectron spectroscopy (UPS) to determine the valence band energy (E_V) of $CuCo_2O_4$ nanotubes, which was calculated to be 7.1 eV by subtracting the width of the He I UPS spectra (Figure 2e) from the excitation energy (21.22 eV). The conduction band (E_B) of $CuCo_2O_4$ estimated at 5.74 eV from $E_V - E_g$, where the E_g is 1.36 eV.

The apparent quantum efficiency (AQE) measurement. A 300-W Xe arc lamp was used as the light source for photocatalytic reaction. The measure ment of AQE was performed using same amount of reactants.

We fixed the wavelength at a certain value for Vis irradiation, the laser power in the photocatalytic reaction was collected using a power meter (Newport; 843-R). The corresponding wavelength captured for AQE calculation is located at the certain value. Thus, the AQE was calculated as the following equation, AQE =n/np × 100 %, in which n and np were denoted as the number of photons that generating product needed and the number of incident photons, respectively.

The apparent quantum efficiency (AQE) calculation.

Under visible light irradiation (450 ± 10 nm) for catalysts within 30 mins, The average intensity of irradiation was found to be 0.0443 W (P1) and 0.038W (P2) before and after the catalyst added to reaction flask by a power meter (Newport; 843-R). The total absorb light energy $\Delta E = (P1-P2)\times t = (0.0443 -$

0.038) × 30 × 60 = 11.34 J,
n =0.0077× 4 mmol = 0.0308 mmol, Energy per photon $E_0 = hc/\lambda = 6.63 \times 10^{-34} \times 3 \times 10^8/(450 \times 10^{-9}) = 4.42 \times 10^{-19}$ J,
Molar of photons np =$\Delta E/(E_0 \times NA) = 11.34/(4.42 \times 10^{-19} \times 6.02 \times 10^{23}) = 4.26 \times 10^{-5}$ mol = 0.0426 mmol, AQE (initial) = n/np =0.0308/0.0426 × 100% = 72%.Using the same method, we can calculate the initial AQE for other catalysts and under other wavelength, respectively.

Photoelectrochemical measurement.

Photoelectrochemical properties were performed on an electrochemical station (CHI 760E) in a standard three-electrode, single-compartment quartz cell. The $CuCo_2O_4$/ITO electrode with an active area of 1 cm^2 served as the working electrodes. The counterelectrode and reference electrode consisted of a platinum sheet (99.99 %, 0.1 mm, 1 cm*2 cm) and Ag/AgCl, respectively. A 300 W Xe lamp with an ultraviolet filter (λ>420 nm) was used as the visible light source and was positioned 10 cm away from the photoelectrochemical cell. Impedance measurements were collected under visible light illumination (λ>420 nm filter, 300 W Xe lamp) in a 0.5 M Na_2S solution at open circuit voltage over a frequency range from 10^5 to 10^{-1} Hz with an AC voltage at 5 mV. The Mott– Schottky plots were obtained at a fixed frequency of 1 kHz to determine the flat-band potential and carrier density. The transient photocurrent was measured using a 20 s on–off cycle at a bias voltage of 0.8 V.

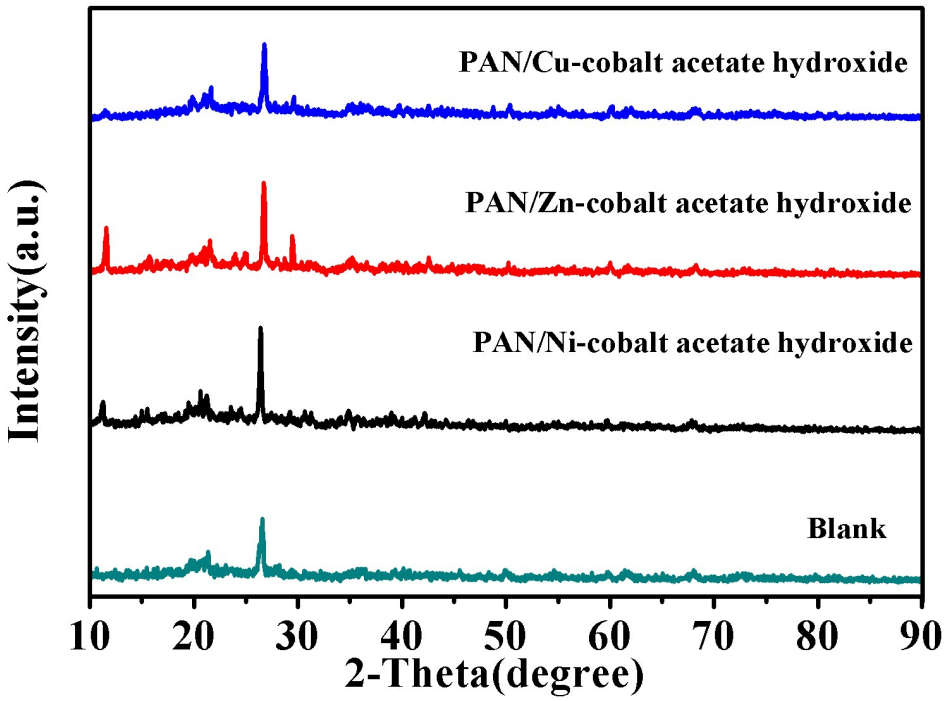

Fig. S1. XRD of PAN/M-Co acetate hydroxide. The blank is the XRD of daub which is used for immobilization samples. The peaks at about 11.58 in the XRD patterns can be well indexed to plane reflections of the M-Co acetate hydroxide, which proved the formation of corresponding basic acetate. [1]

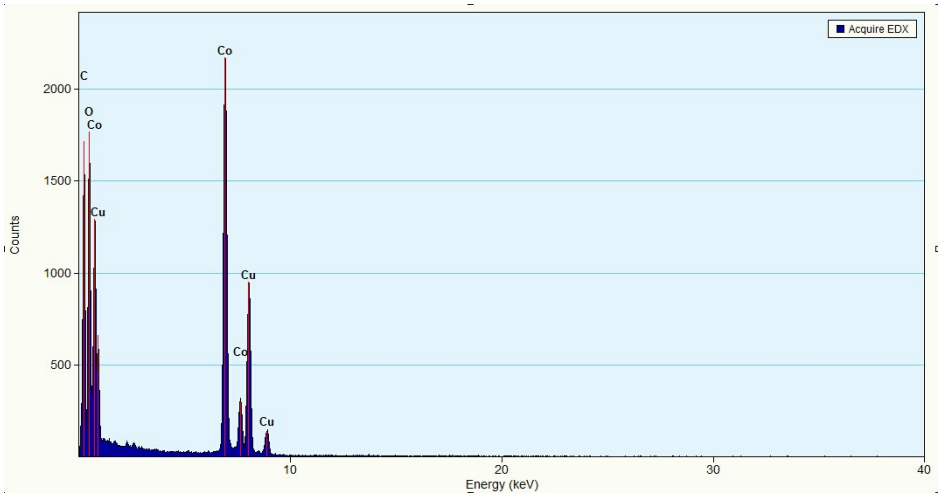

Fig. S2. EDX of nanosheets constructed $CuCo_2O_4$ nanotubes.

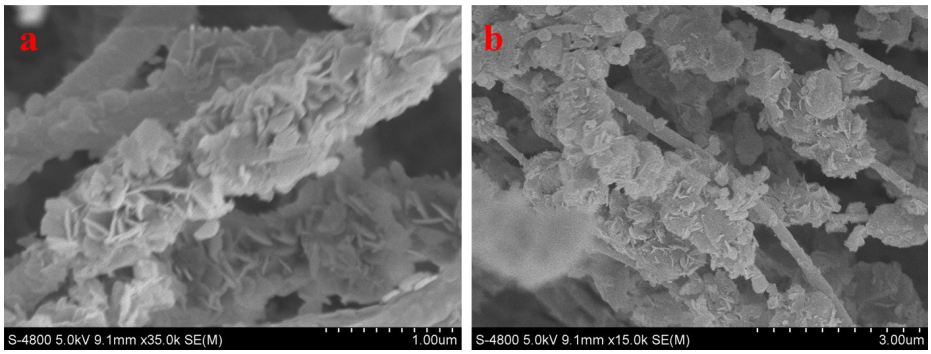

Fig. S3. SEM of PAN/Cu-cobalt hydroxide synthesised by soaking PANCu-Co acetate hydroxide into 1 M KOH (a) or NaOH (b) solution for 2h.

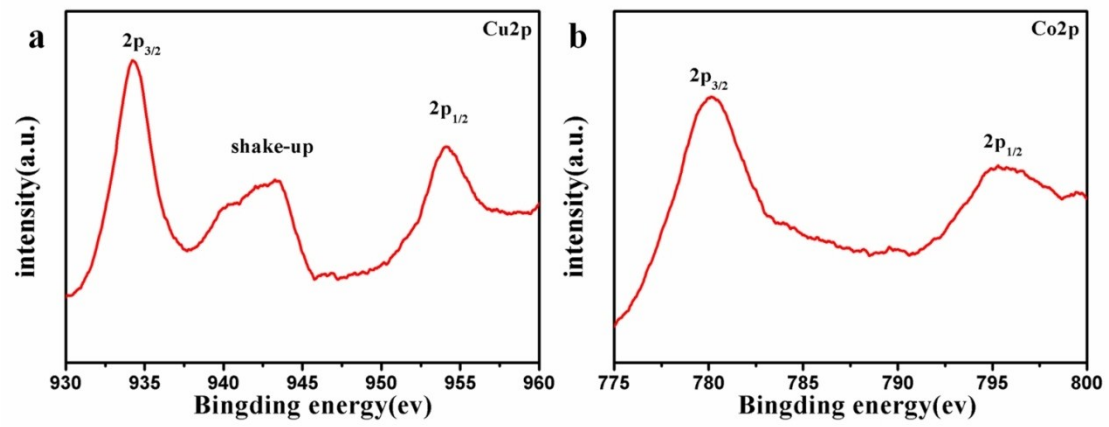

Fig. S4. a) Cu2p XPS spectrum of nanosheets constructed $CuCo_2O_4$ nanotubes; b) Co2p XPS spectrum of nanosheets constructed $CuCo_2O_4$ nanotubes. The X-ray photoelectron spectroscopy (XPS) spectra illustrated in Figure 2a demonstrates the existence of Co, Cu and O in the nanosheets constructed $CuCo_2O_4$ nanotubes. As observed in **Figure S4a**, two peaks at binding energies of 934 and 954 eV in Cu 2p XPS spectra could be assigned to Cu 2p3/2 and Cu 2p1/2, together with a spin-energy separation of around 20 eV. Meanwhile, an additional satellite peak at ~940-944 eV is also observed, confirming the characteristic of Cu^{2+}.[2] As for Co peaks, the binding energies located at ~780 and ~795.4 eV can be assigned to Co 2p3/2 and Co 2p1/2 (**Figure S4b**), together with a spin-energy separation of around 15.4 eV, demonstrating the presence of Co^{3+}.[3]

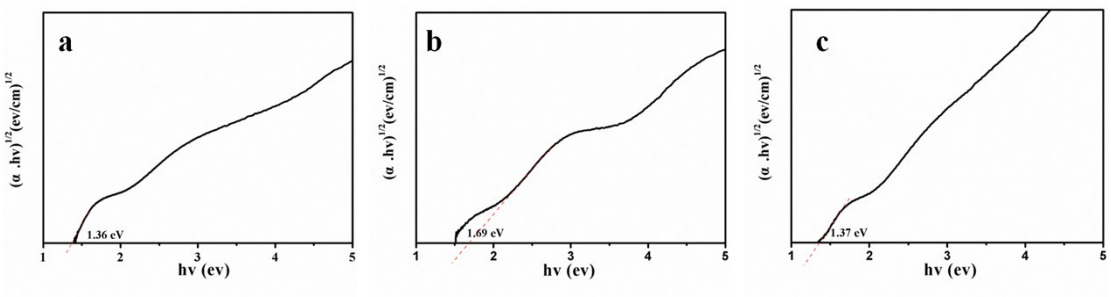

Fig. S5. Tauc plots of nanosheets constructed $CuCo_2O_4$ nanotubes (a), nanosheets constructed $ZnCo_2O_4$ nanotubes (b) and nanosheets constructed $NiCo_2O_4$ nanotubes (c). The band gap energies of nanosheets constructed $CuCo_2O_4$, $ZnCo_2O_4$ and $NiCo_2O_4$ hollow nanotubes are 1.36 eV, 1.69 eV and 1.37 eV, respectively.

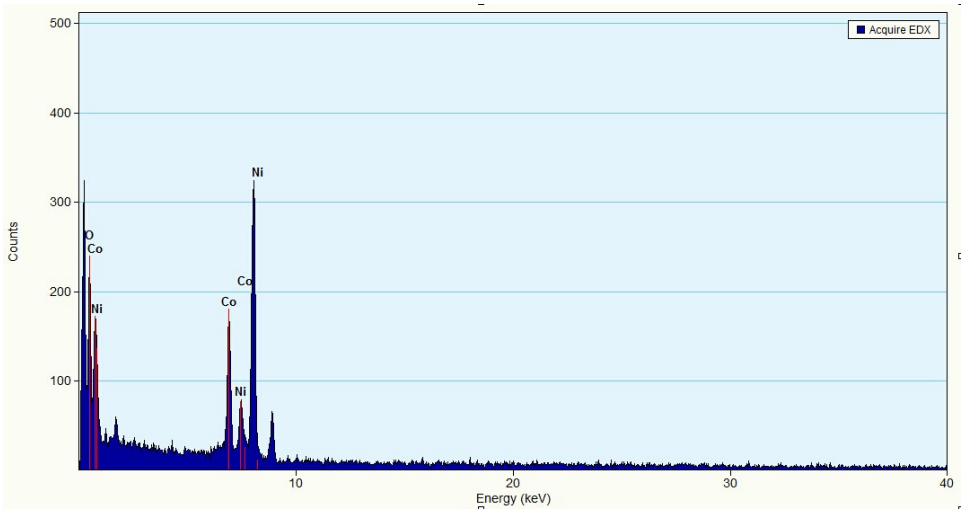

Fig. S6. EDX of nanosheets constructed $NiCo_2O_4$ nanotubes.

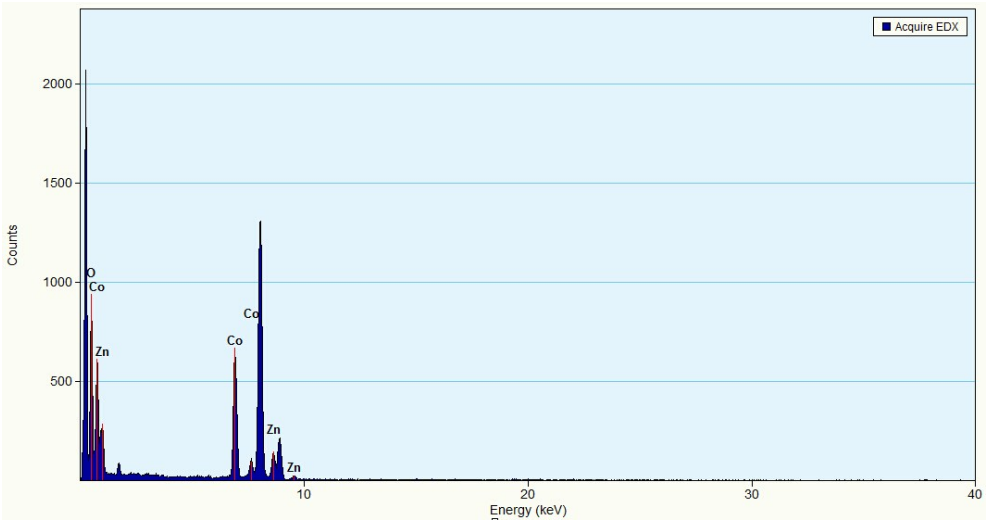

Fig. S7. EDX of nanosheets constructed $ZnCo_2O_4$ nanotubes.

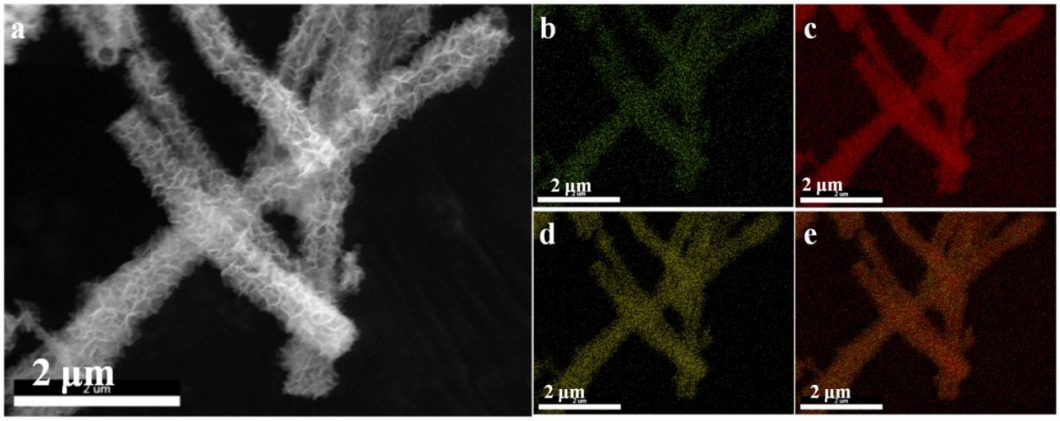

Fig. S8. a) SEM and distribution of element Ni (b), Co (c), O (d) and the overlap (e) in nanosheets constructed $NiCo_2O_4$ nanotubes. The elemental mapping analysis further demonstrates the homogeneous dispersion of Ni, Co, and O elements in nanotubes.

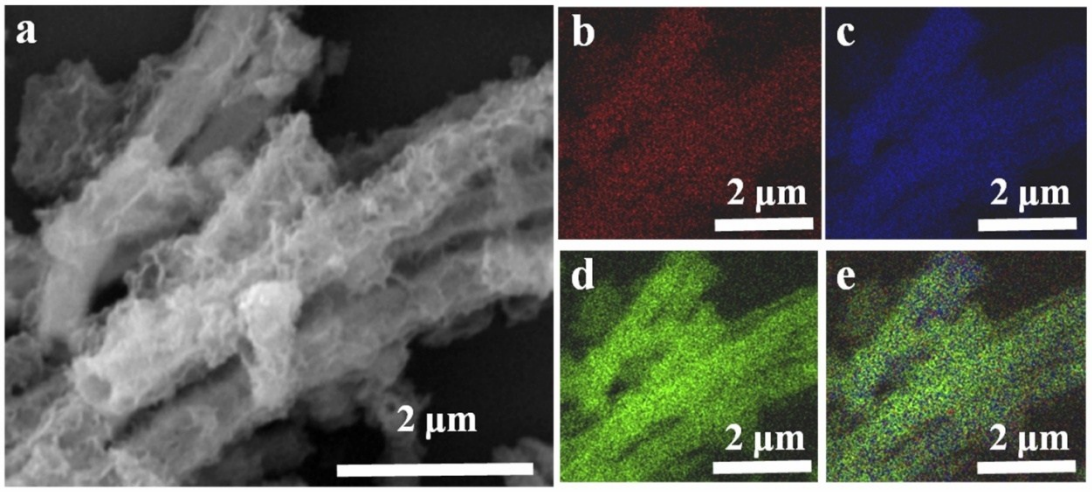

Fig. S9. a) SEM and distribution of element Zn (b), Co (c), O (d) and the overlap (e) in nanosheets constructed $ZnCo_2O_4$ nanotubes. The elemental mapping analysis further demonstrates the existence and homogeneous dispersion of Zn, Co, and O elements in $ZnCo_2O_4$ nanotubes.

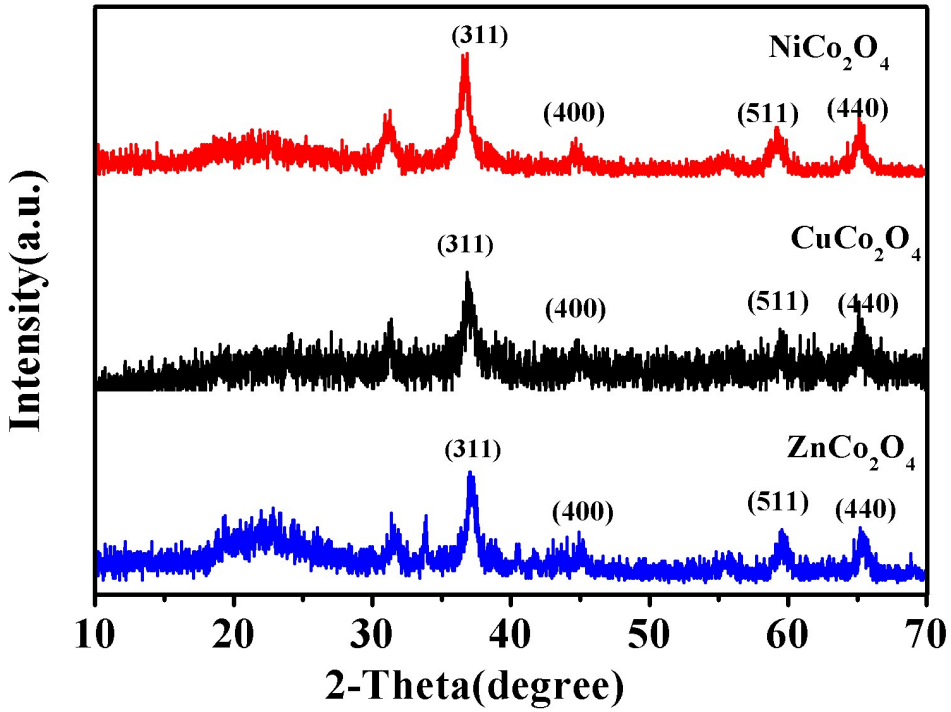

Fig. S10. XRD of nanosheets constructed $CuCo_2O_4$ nanotubes, nanosheets constructed $ZnCo_2O_4$ nanotubes and nanosheets constructed $NiCo_2O_4$ nanotubes. Figure S14 shows the XRD patterns of the as-synthesized nanosheets constructed MCo_2O_4 nanotubes. The diffraction peaks in the XRD pattern can be well indexed to (311), (400), (511), and (440) plane reflections of the spinel $CuCo_2O_4$ phase (PDF#01-1155), $NiCo_2O_4$ phase (PDF#20-0781) and $ZnCo_2O_4$ phase (PDF#23-1390).

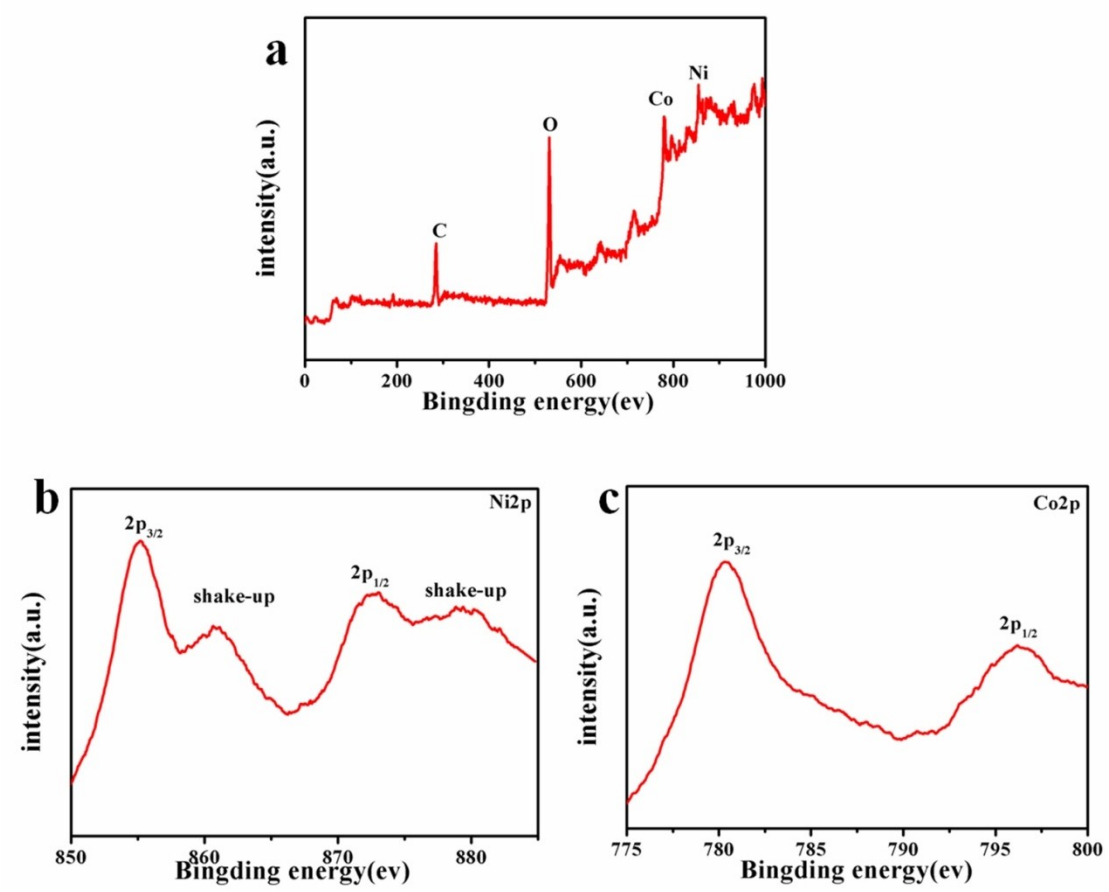

Fig. S11. a) X-ray photoelectron spectroscopy (XPS) spectra of nanosheets constructed $NiCo_2O_4$ nanotubes; b) Ni 2p XPS spectrum of the $NiCo_2O_4$ nanotubes; c) Co2p XPS spectrum of the nanosheets constructed $NiCo_2O_4$ nanotubes. The X-ray photoelectron spectroscopy (XPS) spectra illustrated in Figure S13 demonstrates the existence of Co, Cu and O in the $NiCo_2O_4$ nanotubes. As observed in Figure S15b,Two peaks at binding energies of 856.2 and 874 eV in Cu 2p core (**Figure 11b**) could be assigned to Ni 2p3/2 and Ni 2p1/2, together with a spin-energy separation of around 17.8 eV. Two additional satellite peaks at about 6.2- and 6- ev higher binding energy, confirming the characteristic of Ni^{2+}.[4] As for Co peaks, the binding energies located at ~780 and ~795.4 eV can be assigned to Co 2p3/2 and Co 2p1/2 (**Figure S11c**), together with a spin-energy separation of around 15.4 eV, demonstrating the presence of Co^{3+}.[3]

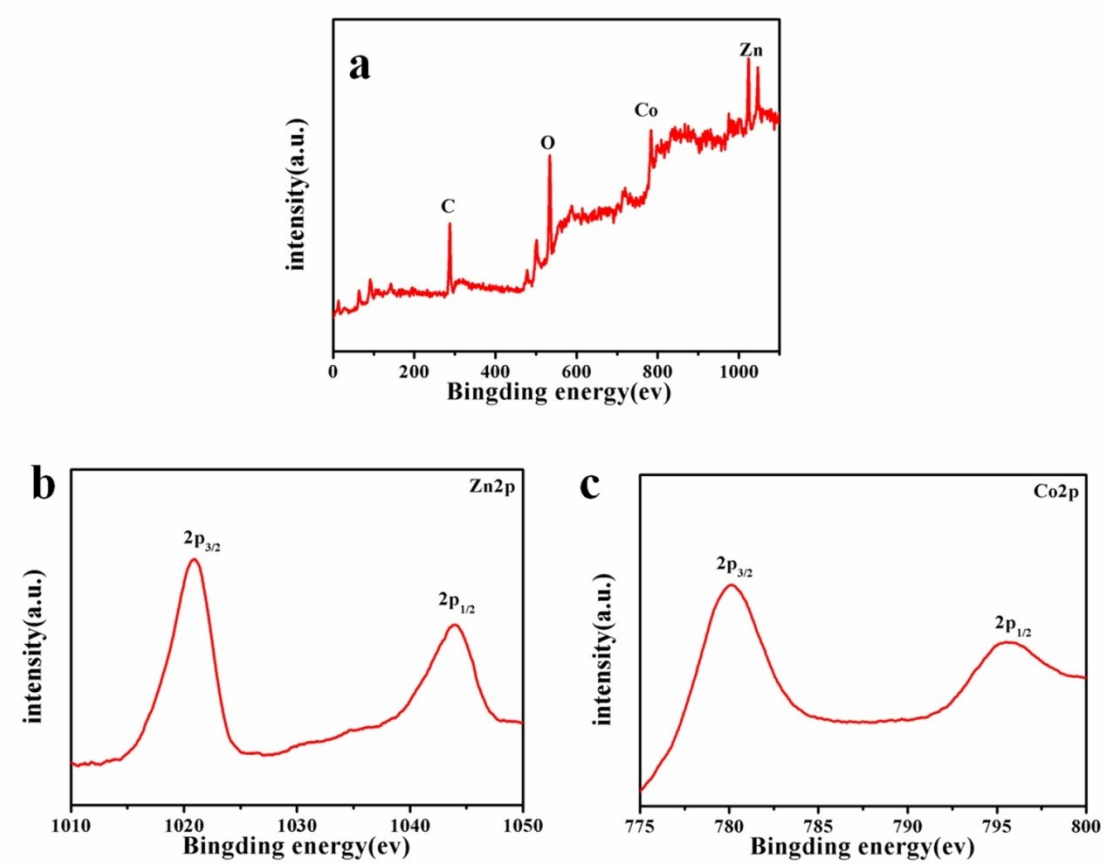

Fig. S12. a) X-ray photoelectron spectroscopy (XPS) spectra of nanosheets constructed $ZnCo_2O_4$ nanotubes; b) Zn2p XPS spectrum of the nanotubes; c) Co2p XPS spectrum of the nanotubes. The X-ray photoelectron spectroscopy (XPS) spectra illustrated in **Figure S12** demonstrates the existence of Co, Zn and O in the nanosheets constructed $ZnCo_2O_4$ nanotubes. As observed in Figure S14b, two peaks at binding energies of 1021 and 1044 eV in Zn 2p XPS spectra could be assigned to Zn 2p3/2 and Zn 2p1/2, confirming the characteristic of Zn^{2+}.[5] As for Co peaks, the binding energies located at ~780 and ~795.4 eV can be assigned to Co 2p3/2 and Co 2p1/2 (**Figure S12c**), together with a spin-energy separation of around 15.4 eV, demonstrating the presence of Co^{3+}.[3]

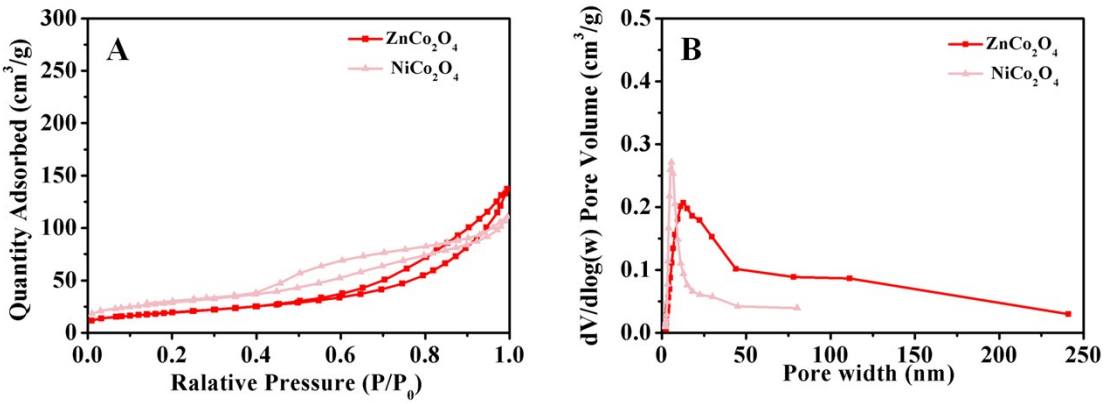

Fig. S13. A) N_2 adsorption/desorption isothermals of nanosheets constructed $NiCo_2O_4$ nanotubes and nanosheets constructed $ZnCo_2O_4$ nanotubes. B) Pore size distributions of nanosheets constructed $NiCo_2O_4$ nanotubes and nanosheets constructed $ZnCo_2O_4$ nanotubes. Nitrogen adsorption measurements revealed that the three kinds of products exhibit the type IV isotherm behavior with H_3 hysteresis, implying that the obtained catalysts are mesoporous. In addition, the specific surface areas of N nanosheets constructed $NiCo_2O_4$ nanotubes determined to be 101 m^2 g^{-1} by Brunauer-Emmett-Teller (BET) analysis and the BET of nanosheets constructed $ZnCo_2O_4$ nanotubes can reach 68.8 m^2 g^{-1}. The distribution of main Barrett-Joyner-Halenda (BJH) pore sizes determined from the adsorption branches are range of 10-25 nm and 10-50 nm for $NiCo_2O_4$ nanotubes and nanosheets constructed $ZnCo_2O_4$ nanotubes, respectively.

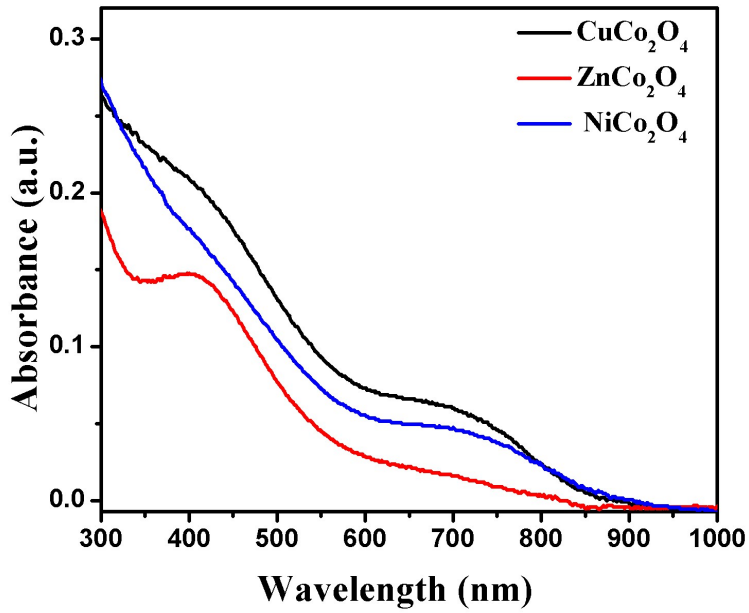

Fig. S14. Uv-vis spectras of nanosheets constructed MCo_2O_4 nanotubes.

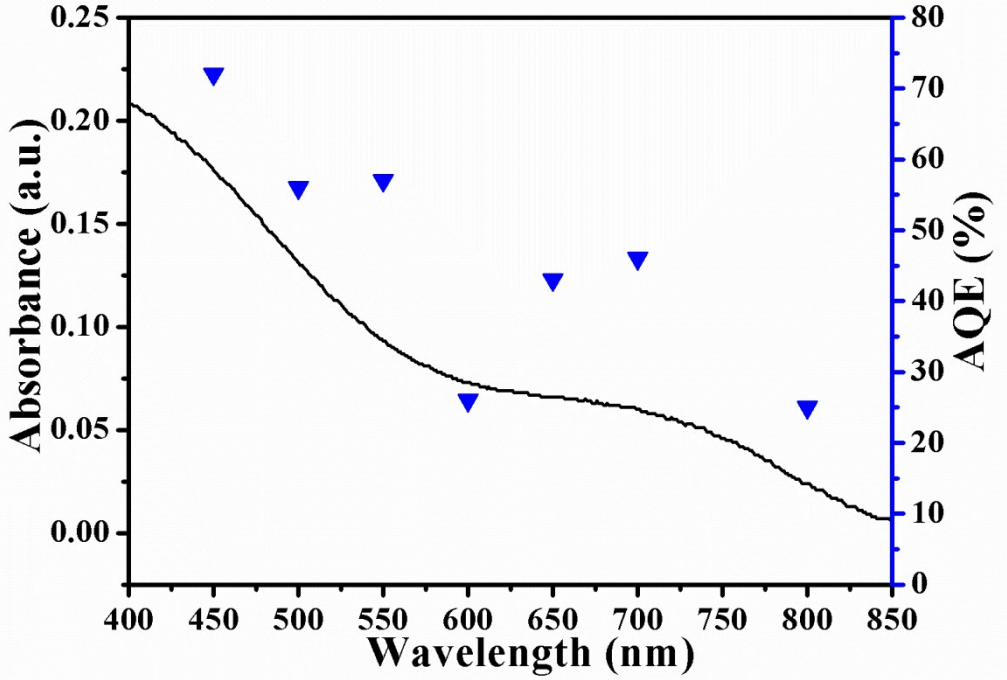

Fig. S15. Uv-vis spectras and apparent quantum efficiency(AQE) of nanosheets constructed $CuCo_2O_4$ nanotubes. The AQE of different wavelength is differen. The AQE estimated between 450 and 850 nm correlates well with the estimated absorbance of the nanosheets constructed $CuCo_2O_4$ nanotubes. The highest AQE is 72% with 450 nm lightting, while the lowest is 25% under 800 nm irradiation, which shows poor absorption which is also higher than some catalyst repaoted , which account for why the $CuCo_2O_4$ nanosheets constructed $CuCo_2O_4$ nanotubes perform high catalytic rate and effciency.

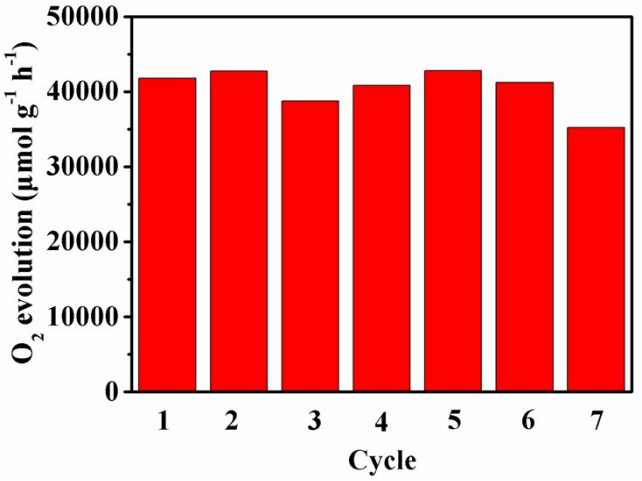

Fig. S16. The corresponding TOF of nanosheets constructed $CuCo_2O_4$ nanotubes in cyclic test. To verify the stability and reliability of catalysts, the nanosheets constructed $CuCo_2O_4$ nanotubes were used for cyclic test and 0.12 g $Na_2S_2O_8$ was

added for each cycle. As shown in Figure S20, the nanosheets constructed $CuCo_2O_4$ hollow nanotubes displayed amazing stability. After seven times used, the TOF and O_2 yield can reach up to 35.2 mmol g^{-1} h^{-1} and 88.8 %, respectively.

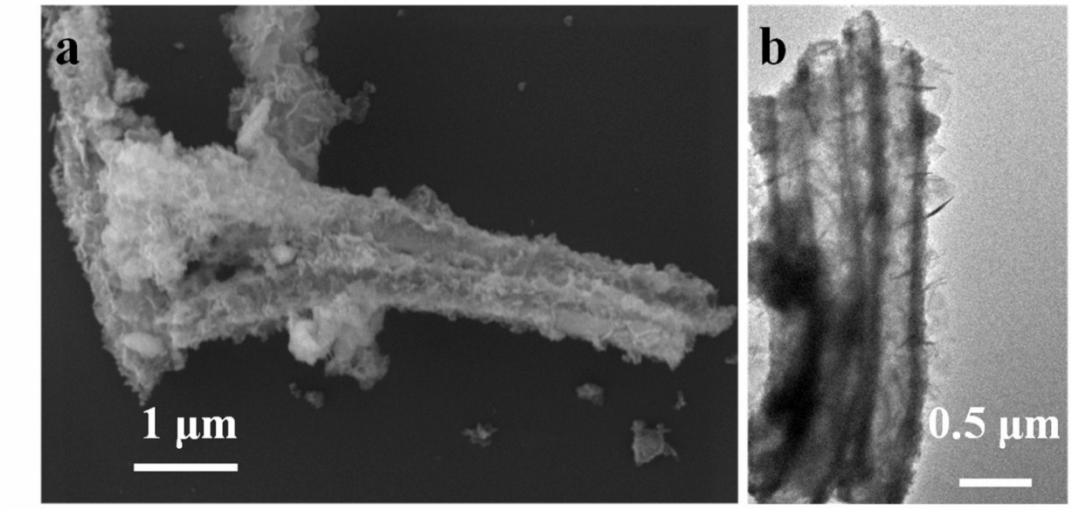

Fig. S17. a) SEM and b) TEM of nanosheets constructed $CuCo_2O_4$ nanotubes after the seventh cycles tests. Compared to the nanosheets constructed $CuCo_2O_4$ nanotubes before tests, the catalyst still keep original appearance although a small amount of collapse, which means the catalyst has good stability.

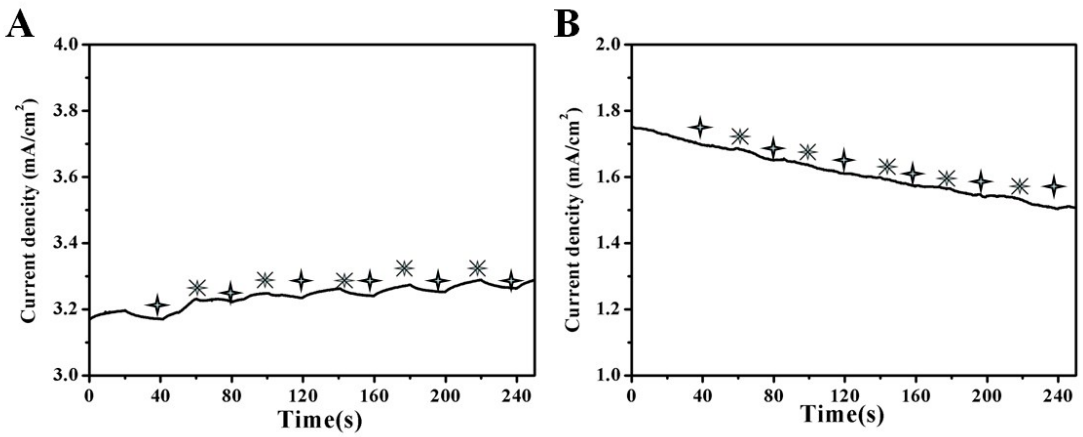

Figure S18. Currents with and without illumination, by $ZnCo_2O_4$/ITO (A) and $NiCo_2O_4$/ITO (B) glass in 0.5 M Na_2S solution at 0.8 V vs. Ag/Ag Cl. Stars signify "light on". Stars with crosses through them indicate "light off". As shown in Figure S21, the current density of $ZnCo_2O_4$/ITO and $NiCo_2O_4$/ITO glass is not improved obviously under illumination. The $ZnCo_2O_4$ and $NiCo_2O_4$ exhibited little photocurrent responses.

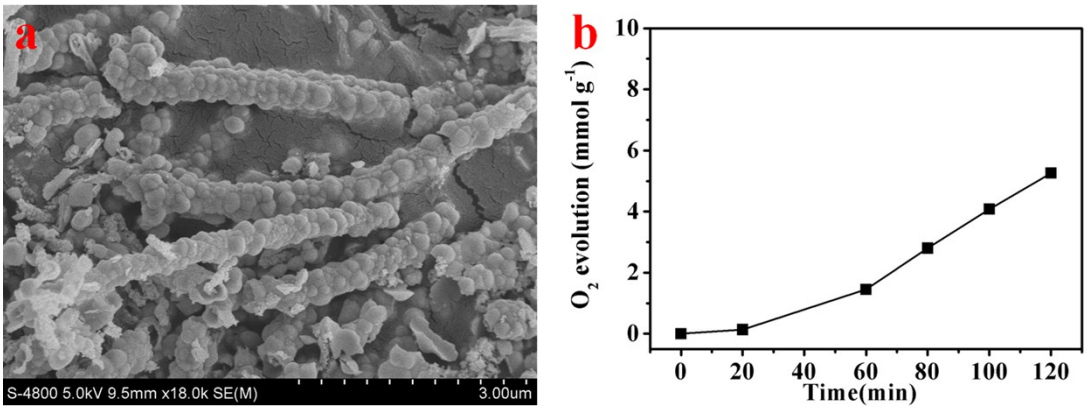

Figure S19. a) SEM image and b) Oxygen evolution performance of $CuCo_2O_4$ nanofibers through processing the PAN@Cu-Co acetate hydroxide by a calcination method in air atmosphere, under visible light irradiation ($\lambda > 420$ nm). As shown in Figure S19a, without $NaBH_4$, nanosheets constructed nanotubes can not be prepared through processing the PAN@Cu-Co acetate hydroxide by a calcination method in air atmosphere. As shown in Figure S19 and Figure 4a, nanosheets constructed $CuCo_2O_4$ nanotubes present higher catalytic actvity (51.1 $mmolg^{-1}h^{-1}$) than $CuCo_2O_4$ catalyst (2.6 $mmolg^{-1}h^{-1}$) through processing the PAN@Cu-Co acetate hydroxide by a calcination method in air atmosphere**.**

Sample	**Actual Metal** (wt %)	**Co/M ratio**
$CuCo_2O_4$	**12.7(Cu):22.7(Co)**	1.97:1
$NiCo_2O_4$	**20.0(Ni):37.6(Co)**	1.87:1
$ZnCo_2O_4$	**20.9(Zn):35.6(Co)**	1.91:1

Table S1. Elemental analyses of the prepared nanosheets constructed MCo_2O_4 nanotubes.

References.

1 Y. Chen, Z. Li, X. Lou, *Angew. Chem. Int. Ed.,* 2015, **54**, 10521-10524.

2 K. Koski, J. Cha, B. Reed, C. Wessells, D. Kong, Y. Cui, *J. Am. Chem. Soc.,* 2012, **134**, 7584-7587.

3 G. Wang, X. Deng, D. Gu, K. Chen, B. Spliethoff, H. Bongard, C.Weidenthaler, W. Schmidt, F. Schuth, *Angew. Chem. Int. Ed.,* 2016, **55**, 11101-11105.

4 B. Hoffer, A. Langeveld, J. Janssens, R. Bonn6, C. Lok, J. Moulijn, *Journal of Catalysis*, 2000, **192**, 432-440.

5 S. Hwang, J. Song, Y. Jung, O. Kweon, H. Song, J. Jang, *Chem. Commun.,* 2011, **47**, 9164-9166.